Indonesian Journal of Science & Technology

Journal homepage: http://ejournal.upi.edu/index.php/ijost/

Microstructure and Wear Behavior of Repair Weld on the Flash-Butt Welded Rail

*Hein Zaw Oo, Prapas Muangjunburee**

Prince of Songkla University, Hat Yai, Songkhla, Thailand
*Correspondence: E-mail: prapas.m@psu.ac.th

ABSTRACT

This study aimed to evaluate the potential of using a standard arc welding process to repair surface defects in flash-butt welded (FBW) rails by examining their microstructural, mechanical, and tribological properties. Macrostructural analysis, optical microscopy (OM), field emission scanning electron microscopy (FESEM), hardness testing, and wear tests were employed to compare original and repaired FBWs. The repaired weld revealed fine pearlite in the heat-affected zone (HAZ) and acicular ferrite in the weld metal, while hardness results indicated a higher and more uniform distribution across the weld metal and HAZ than in the original FBW. Wear tests showed that both welds had similar coefficients of friction and wear track widths, but the repaired FBW demonstrated less weight loss. SEM analysis identified micro-ploughing and micro-cutting as dominant wear mechanisms in the original FBW, whereas the repaired FBW primarily exhibited micro-ploughing and oxide delamination. These findings indicate that arc welding repair not only improves hardness uniformity but also enhances wear resistance without significantly affecting frictional behavior. In conclusion, the arc welding process can be considered an effective method for restoring the surface integrity of FBW rails, with the implication that its application in rail maintenance may extend rail service life and reduce replacement costs.

ARTICLE INFO

Article History:
Submitted/Received 02 May 2025
First Revised 29 Jun 2025
Accepted 26 Aug 2025
First Available Online 27 Aug 2025
Publication Date 01 Sep 2026

Keyword:
Flash-butt Rail Welding,
Hardness,
Rail Steel,
Repair Welding,
Wear.

1. INTRODUCTION

Currently, welded rail tracks are widely used in most modern railway systems. These tracks make it possible to join rail ends, producing a continuous rail that can extend for many kilometers. In recent years, the application of welding techniques for rail joining has become a global standard practice [1]. Welded tracks provide several advantages, including allowing trains to operate at higher speeds, reducing friction at the wheel–rail interface, and lowering overall energy consumption [2]. As an essential component of the wheel–rail system, welded rails ensure the safe and efficient operation of trains. The increasing demand for high-speed transportation has further driven the development and adoption of continuous welded tracks, which are formed by joining rail segments through welding [3]. However, there is a significant difference between the rail steel and the weld metal in terms of microstructure and mechanical properties. These differences, caused by microstructural inhomogeneity during the welding process, lead to susceptibility to wear in both the rail and the weld region [4].

The two main welding techniques currently used for joining rails are thermite welding and flash-butt welding. Thermite welding relies on an exothermic reaction that produces molten steel, which is then poured into a mold cavity to join the rail ends [5]. In contrast, flash-butt welding employs an electric current to heat the rail ends before they are pressed together and forged into a solid weld [6]. In general, the failure rate of flash-butt welds is lower than that of thermite welds [7,8]. Compared with flash-butt welds, thermite welds are typically wider and more prone to internal defects due to the nature of the welding process. Several drawbacks of thermite welding include the frequent formation of weld defects and a greater reduction in strength, which make the welds more susceptible to rolling contact fatigue (RCF) defects resulting from the larger weld zone and heat-affected zones (HAZs). For these reasons, flash-butt welding has been increasingly adopted as a replacement for thermite welding in modern railway systems [9].

During the track installation process, flash-butt welding is employed to connect shorter rail segments into longer sections, typically around 400 meters in length [1]. It is estimated that flash-butt welding accounts for approximately 80% of welded rail joints because of its ability to provide greater stability and higher-quality welds [10]. Moreover, flash-butt welding has gained popularity in the production of welded rails, which enhance the dynamic performance of railways and ensure longer service life [11]. Although welded rails are generally more durable than non-welded rails, there remains a risk of weld failure due to variations in the microstructure and mechanical properties of the parent rail [12]. The heat-affected zones (HAZs) of welded rail joints typically exhibit reduced mechanical properties, such as lower hardness, strength, and wear resistance [13,14]. Consequently, the welded joint often becomes a weak point in the track structure, making it more vulnerable to damage under service conditions [15,16].

Welding induces rapid localized heating, which generates steep temperature gradients and produces nonequilibrium cooling conditions. These gradients influence the base metal, with the temperature decreasing progressively as the distance from the fusion line increases. As a result, different regions of the welded joint develop inhomogeneous microstructures [17]. Another critical consequence is the reduction of mechanical properties in the heat-affected zone (HAZ), caused by changes in eutectoid morphology due to the uneven temperature distribution during welding. In the partial austenitization region, the eutectoid transformation alters the pearlitic structure into spheroidized cementite dispersed within a ferritic matrix. This transformation decreases hardness and, consequently, accelerates localized wear.

DOI: https://doi.org/10.17509/ijost.v11i2.89691
p- ISSN 2528-1410 e- ISSN 2527-8045

The heat input from flash-butt welding provides sufficient energy for phase transformations to occur in the heat-affected zone (HAZ) [18]. Nishikawa and Goldenstein demonstrated that the region with reduced hardness and a spheroidized carbide microstructure, formed in the HAZ during welding, corresponds to the partial austenitization zone [19]. In this region, a divorced eutectoid transformation occurs. The relatively low austenitizing temperature prevents the complete dissolution of spheroidal cementite particles, which then act as nucleation sites for eutectoid phase transformation during cooling. Consequently, the decomposition of austenite produces a ferritic matrix containing dispersed spherical cementite.

In the heat-affected zone (HAZ) of a welded rail joint, regions with lower hardness generally exhibit lower yield strength, making them more susceptible to plastic deformation under wheel–rail contact and thus increasing the risk of damage. This occurs because, in rail steels, yield strength is approximately three times the hardness value [20]. The reduction in hardness caused by cementite spheroidization within the HAZ, resulting from partial austenitization, presents a critical challenge for the railway industry [21]. Over the service life of a railway, variations in hardness within flash-butt welded (FBW) rail heads may lead to localized wear [22]. Furthermore, the mechanical strength of FBW joints can be compromised by microstructural changes occurring in both the weld centerline and the HAZ. Previous studies have shown that cementite spheroidization in these regions causes a localized reduction in tensile strength [13]. Porcaro et al. investigated the flash-butt welding process and mechanical performance through tensile tests on both the entire weld zone and the base metal at the specimen center, reporting a reduction in yield stress with fractures occurring in the partial austenitization and pearlite spheroidization regions [21]. Similarly, Fegredo et al. demonstrated that partial spheroidization of cementite in pearlite increases the wear rate and alters the plastic flow behavior on rail surfaces, while also reducing the yield strength and hardness of the original steel [23].

Localized rolling contact fatigue (RCF) problems, including squats, have been observed on the centerline and heat-affected zone (HAZ) of flash-butt welded rail head surfaces, with a high concentration at the gauge corner of high rails [9]. Mutton et al. reported that in flash-butt welded pearlitic rails, RCF cracks preferentially initiate and propagate within specific microstructural features [24]. Their study showed that fatigue fractures propagated rapidly and were consistently located within spheroidization zones on either side of the HAZ. They further emphasized that softened areas are particularly vulnerable to RCF crack initiation, especially at the gauge corner. Liu et al. examined the rolling contact wear mechanism of U75V rail flash-butt welded joints using a double-disc rolling test across different regions of the joint, including the bonding line (BL), HAZ, and softening zone (SZ). Their findings demonstrated that each region of the welded joint exhibits a distinct wear mechanism, which can be directly attributed to its unique microstructural characteristics.

For decades, squats have posed a major challenge to railway systems worldwide, threatening both operational safety and the long-term durability of rails. Even a single squat defect has the potential to evolve into a catastrophic rail fracture, thereby endangering passenger safety. Single squats often occur at the center of flash-butt welded (FBW) joints, whereas duo squats are typically found on either side of the heat-affected zone (HAZ) in thermite weld joints [25]. Importantly, the weakness of FBW joints lies not only in the HAZ but also in the weld centerline. Consequently, defects that appear on the rail running surface must be repaired promptly to prevent propagation and the formation of cracks. The HAZ of welded rail joints is the most common site of surface defects such as spalling and squats. To minimize defects by reducing the width of the spheroidized region. However, this approach

DOI: https://doi.org/10.17509/ijost.v11i2.89691
p- ISSN 2528-1410 e- ISSN 2527-8045

often results in the formation of brittle phases such as martensite and increases tensile residual stress in the web region, which can ultimately cause rail failure at welded joints under high axle loads [18].

The defect removal methods currently employed by the railway industry are both costly and time-consuming. Therefore, repair strategies for surface defects such as squats in flash-butt welded rails must emphasize practicality, cost-effectiveness, safety, and ease of field application. When damage or wear occurs on the surface of a welded rail joint, appropriate repair treatment is required to extend its service life and improve durability. A multi-pass slot welding technique as a suitable solution for repairing railhead defects. This method involves accurately identifying and removing the defective region by machining a perpendicular slot that encompasses the defect, followed by welding. Furthermore, previous studies have demonstrated that the softened regions in the HAZ of thermite welded joints, characterized by spheroidized microstructures, can be effectively repaired and enhanced using a standard arc welding process [26,27].

In recent years, considerable attention has been directed toward improving the quality of flash-butt welded rails, particularly due to concerns about hardness reduction within the heat-affected zones (HAZs) [28]. However, the application of conventional arc welding as a method to repair surface defects in flash-butt welded rail joints has not yet been thoroughly investigated. It is proposed that flash-butt welded rail head surface defects on the rail running surface can be repaired using a standard fusion welding process in an efficient and cost-effective manner, without compromising the integrity of the original flash-butt weld or the base rail. Accordingly, this study evaluates repair welds in comparison with original flash-butt welds, focusing on improvements in metallurgical, mechanical, and tribological properties.

2. METHODS

2.1. Welding Procedures of Repair Weld

Standard railway steel grade R260 rails were joined using the flash-butt welding (FBW) process. The detailed parameters of the original flash-butt welded rail joint are presented in **Table 1**. For the repair procedure, a flux-cored arc welding (FCAW) process was employed to fill a groove measuring 30 mm in diameter and 5 mm in depth, machined at the center of the flash-butt welded rail head surface. The size and location of the groove are illustrated in **Figure 1**. The repair was carried out using a commercial pearlitic welding wire with a diameter of 1.6 mm, while pure carbon dioxide served as the shielding gas. The chemical compositions of the base rail steel and the repair welding electrode are provided in **Table 2**. Before welding, the groove was preheated to 500 °C. Two primary conditions were investigated in this study: the original flash-butt welded joint, which is referred to as the “original FBW,” and the repaired joint, in which the machined groove shown in **Figure 1** was filled using the FCAW repair weld, referred to as the “repaired FBW.” The welding parameters for the repaired FBW are given in **Table 3**.

Table 1. Welding parameters of original flash-butt welded joint.

Flash-Butt Welding Parameters	Values
Duration of burn off (s)	24.00
Flashing current (A)	114.00
Flashing voltage (V)	343.00
Flashing speed (mm/s)	0.19
Duration of preheating (sec)	40.00
Forging force (ton)	47.00
Weld upsetting (mm)	13.10

DOI: https://doi.org/10.17509/ijost.v11i2.89691
p- ISSN 2528-1410 e- ISSN 2527-8045

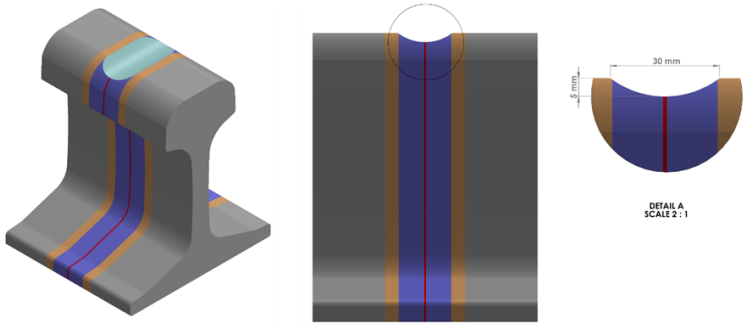

Figure 1. Location of groove to repair the surface defects of flash butt welded rail – weld centerline (red), weld metal (blue), HAZ (yellow) and base rail (grey).

Table 2. Chemical composition of the base rail steel and the repair welding wire electrode.

Materials	C	Si	Mn	P	Mo	Cr	Fe
Rail Steel	0.62-0.8	0.15-0.58	0.7-1.2	<0.025	-	<0.15	Balance
Pearlitic Electrode	0.13	0.64	1.7	-	0.53	0.48	Balance

Table 3. Details parameters of repaired FBW.

Parameters	Current	Voltage	Speed	Heat Input	Gas Flow Rate
Repaired FBW	200-240 A	25 V	40 cm/min	7.5-9 kJ/cm	20 l/min

2.2. Microstructural Characterization

For microstructural examination, specimens were cut vertically across the weld, including a portion of the base rail, along the cross-sectional plane of the rail. The specimen dimensions were sufficiently large to be handled manually, eliminating the need for mounting during preparation. A comparative analysis was conducted between the original FBW and the repaired FBW based on their cross-sectional macrostructures. Both conditions were examined using a Carl Zeiss optical microscope (OM) to observe the optical microstructure. In addition, an FEI field emission scanning electron microscope (FESEM) was employed to analyze the microstructures of the original and repaired FBWs at higher magnifications.

2.3. Microhardness testing

Hardness measurements were carried out across the cross-sections of the samples in several regions. The micro-Vickers hardness of both the original FBW and the repaired FBW was measured at a depth of 3 mm from the running surface. A test load of 200 g with a dwell time of 10 s and a spacing interval of 0.5 mm between indentations was applied. After repair, the hardness distribution at the FBW centerline was specifically evaluated and compared with that of the original FBW.

2.4. Ball-on-disc Wear Testing

The wear behavior of the specimens, before and after repair, was evaluated using an ASTM G99 standard ball-on-disc wear test. Alumina (Al_2O_3) balls with a diameter of 6 mm were used as the counter body. Round specimens measuring 25 mm in diameter and 2 mm in thickness were prepared for testing. During the experiment, a sliding track with a 5 mm radius was subjected to a normal load of 10 N at a sliding speed of 10 cm/s. All tests were conducted at ambient temperature. The weight of each specimen was measured using an electronic scale

DOI: https://doi.org/10.17509/ijost.v11i2.89691
p- ISSN 2528-1410 e- ISSN 2527-8045

before and after testing, and the difference was recorded as weight loss. To ensure reliability, three wear tests were performed for each condition. The surface morphology of the worn specimens was subsequently analyzed using a scanning electron microscope (SEM).

3. RESULTS AND DISCUSSION

3.1. As-repaired Condition

Figure 2 presents the prepared groove on the surface of the original FBW rail. The detailed dimensions and the exact location of the groove on the FBW rail head are illustrated in **Figure 1**. **Figure 2(a)** shows the groove on the FBW rail surface prior to preheating and repair, while **Figure 2(b)** displays the FBW rail surface after repair, where the groove was filled with FCAW weld in the transverse direction of the FBW rail. Following completion of the repair process and subsequent cooling of the rail sample, a visual inspection was conducted to evaluate the quality of the repair weld. No cracks or surface defects were detected, indicating that the repair weld exhibited satisfactory surface quality.

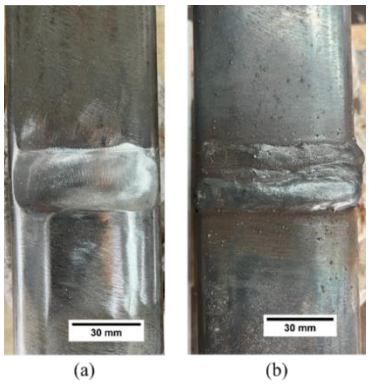

Figure 2. Actual groove of repaired FBW (a) before repair, (b) after repair.

3.2. Macrostructure

Figure 3 shows the macrostructure of the repaired FBW, encompassing the weld metal and the HAZs. After the repair, the weld centerline, weld zones, and the HAZs of the original FBW remained clearly distinguishable. No defects or cracks were observed in the cross-sectional macrostructure. The HAZ of the repair weld was approximately 5 mm wide on both sides. Owing to the size and geometry of the groove, the repair weld metal and its associated HAZs were fully contained within the original flash-butt weld and its HAZs. Furthermore, the base rail steel exhibited no alteration after the top surface of the FBW joint was repaired.

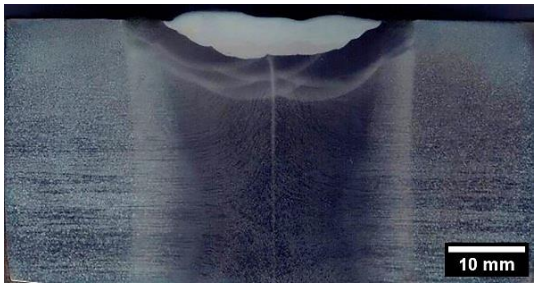

Figure 3. Macrostructure of repaired FBW's rail head.

3.3. Optical Microstructure

According to the macrostructural observations, the weld region of the original FBW can be divided into three distinct zones: the weld centerline, the weld metal, and the HAZ. The

DOI: https://doi.org/10.17509/ijost.v11i2.89691
p- ISSN 2528-1410 e- ISSN 2527-8045

optical microstructure of the weld centerline is presented in **Figure 4(a)**. In this region, proeutectoid ferrite is observed along the grain boundaries, which can be attributed to the exposure to high temperatures followed by a rapid cooling rate. The microstructure of the weld metal, shown in **Figure 4(b)**, primarily consists of pearlite. Unlike thermite weld metal, which exhibits dendritic features due to solidification from a liquid state, the FBW joint does not display such cast microstructural characteristics because FBW is a solid-state welding process. **Figure 4(c)** presents the HAZ microstructure of the original FBW joint, which consists of partially spheroidized cementite embedded within a ferrite matrix.

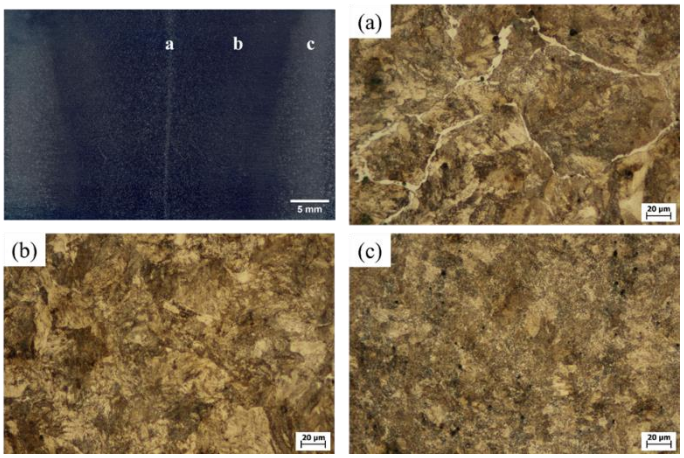

Figure 4. Optical microstructure of the original FBW (a) weld centerline, (b) weld metal, and (c) HAZ.

The optical microstructure of the repaired FBW, including both the weld metal and the HAZ, is presented in **Figure 5**. In the weld metal microstructure **(Figure 5a)**, acicular ferrite phases containing numerous inclusions are observed. Distinguishing between acicular ferrite and bainite under an optical microscope is challenging, as both exhibit similar morphologies [29]. Although their formation processes and temperature ranges overlap, bainite develops through the growth of ferrite in parallel plate structures at the austenite grain boundaries. In contrast, acicular ferrite nucleates on non-metallic inclusions within the grains [30]. Primary acicular ferrite plates, formed in association with inclusions, subsequently serve as nucleation sites for secondary acicular ferrite [31]. The HAZ microstructure of the repaired FBW, shown in **Figure 5(b)**, is predominantly composed of fine pearlite.

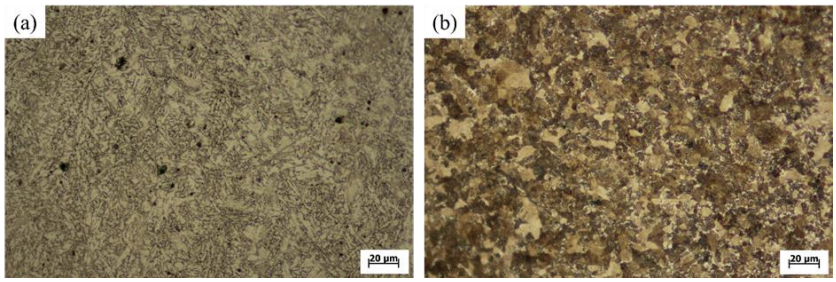

Figure 5. Optical microstructure of repaired FBW (a) weld metal, (b) HAZ.

3.4. Field Emission Scanning Electron Microstructure (FESEM)

Figure 6(a) presents FESEM images of pearlitic rail steel (R260) at different magnifications. In the electron micrograph, cementite appears as the light phase, while ferrite appears as the dark phase [32]. At higher magnification, the lamellar pearlite structure is clearly visible, with nanoscale cementite lamellae embedded in the ferrite matrix characteristic of pearlite. The

DOI: https://doi.org/10.17509/ijost.v11i2.89691
p- ISSN 2528-1410 e- ISSN 2527-8045

interlamellar spacing of ferrite and cementite was generally measured in the range of 150–300 nm [33]. Such a pearlitic microstructure provides excellent wear resistance under rolling sliding loads [34].

Figure 6(b) shows the microstructure of the flash-butt weld (FBW) metal. Since pearlitic rail steel (R260) was employed in this study, the weld metal also exhibits a pearlitic structure, although with different lamellar spacing compared to the base rail. Specifically, the weld metal displayed finer pearlite lamellae, reflecting the influence of the thermal and mechanical stresses generated during the FBW process.

In **Figure 6(c)**, the weld centerline microstructure is characterized by pearlite with thin lamellae and proeutectoid ferrite phases located along the grain boundaries. The presence of ferrite at grain boundaries can be attributed to the elevated temperature and rapid cooling rate experienced during welding. Near the weld centerline, temperatures approached the melting point of the rail steel during the upsetting stage. Upon cooling, proeutectoid ferrite formed at the austenitic grain boundaries, while the rapid cooling rate restricted sufficient carbon diffusion into the ferrite [12].

Figure 6(d) shows the microstructure of the heat-affected zone (HAZ) in the FBW rail, where a spheroidized microstructure was observed. This region represents a weak point in the FBW rail joint, as the presence of spheroidized cementite significantly affects the overall quality of the weld. Within the HAZ, particularly in the partial austenitization zone, cementite phases undergo spheroidization. At these temperatures, the lamellar cementite of the original pearlite can partially dissolve and subsequently transform into spheroidized cementite due to the relatively slower cooling rate after welding. Compared to the base metal, the spheroidized microstructure exhibits lower hardness, making this region more susceptible to degradation in mechanical performance.

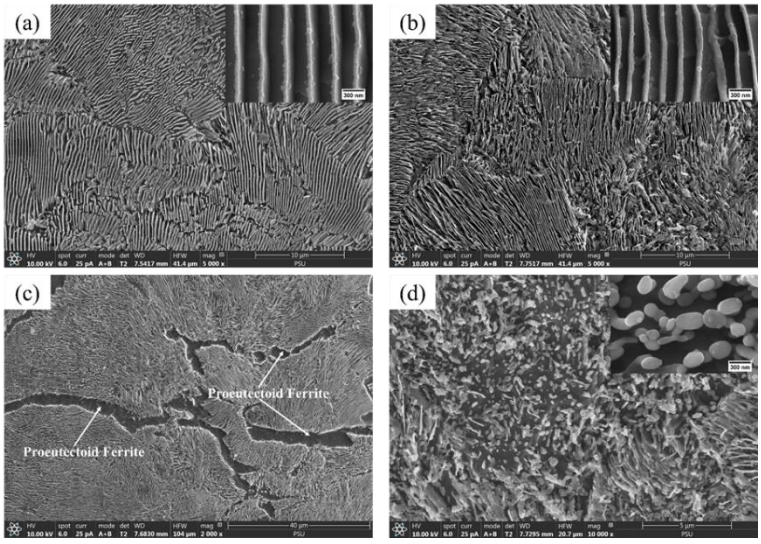

Figure 6. FESEM micrographs of the original FBW (a) base rail steel, (b) weld metal, (c) weld centerline, and (d) HAZ.

In **Figure 7(a)**, the fusion line distinctly separates the weld metal from the heat-affected zone (HAZ) of the repair weld, with the contrasting microstructures across the interface clearly visible. **Figure 7(b)** presents the FESEM micrograph of the repair weld metal, showing the microstructure dominated by acicular ferrite phases, where acicular ferrite plates develop within the grain boundaries in irregular orientations. **Figure 7(c)** illustrates the FESEM microstructure of the repaired FBW's HAZ, which exhibits a finer pearlitic structure characterized by thinner cementite lamellae and narrower lamellar spacing compared to the

DOI: https://doi.org/10.17509/ijost.v11i2.89691
p- ISSN 2528-1410 e- ISSN 2527-8045

base rail steel. The refinement of lamellar spacing plays a critical role in improving wear resistance, as smaller spacing effectively reinforces the ferrite matrix, reduces the thickness of the plastic deformation layer, and enhances surface hardness. This improvement arises from the significant work hardening of ferrite and the accumulation of dislocations constrained by the undivided lamellae, ultimately contributing to the superior wear resistance of the repaired FBW joint [35].

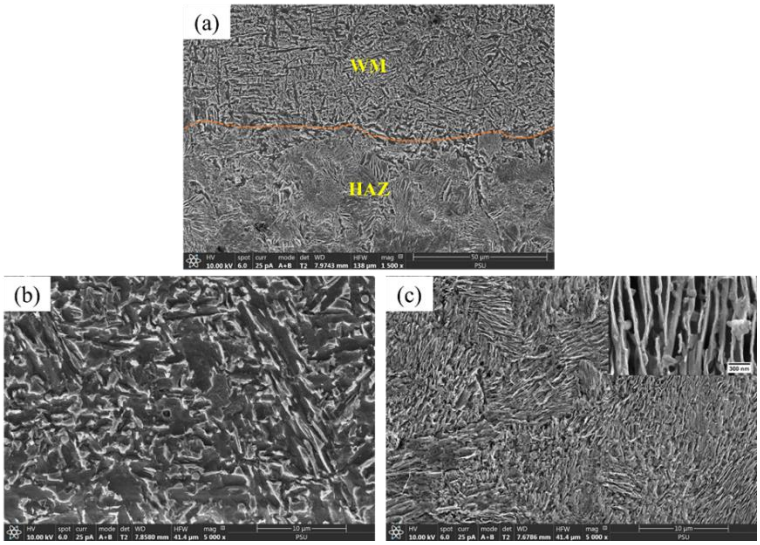

Figure 7. FESEM images of repaired FBW (a) fusion line, (b) weld metal, (c) HAZ.

3.5. Hardness

Figure 8 presents the Vickers hardness profiles of both the original and repaired FBW rails. Hardness measurements were conducted along the weld cross-section, 3 mm beneath the rail surface, extending from the weld centerline toward the base metal on both sides. The yellow curve represents the hardness profile of the original FBW, while the green curve corresponds to the repaired FBW. The red dashed line at 0 mm marks the weld centerline of the original FBW. The weld metal of the original FBW exhibited hardness values ranging from 310 HV to 360 HV, with an average of approximately 340 HV. By comparison, the repaired FBW showed hardness values between 330 HV and 370 HV, averaging around 350 HV. The relatively stable hardness distribution in the repaired FBW indicates a more homogeneous weld metal microstructure, which may be attributed to improved thermal cycles and material redistribution during the repair process. Overall, no significant difference in weld metal hardness was observed before and after repair, although the repaired FBW demonstrated a slightly higher average hardness (about 10 HV) and reduced variability at the weld centerline. Furthermore, the regions that exhibited the greatest reduction in hardness in the original FBW particularly the HAZ and weld centreline showed notable improvement following the repair.

Figure 9 shows the average hardness values of the two HAZ regions in both the original and repaired FBW. The HAZ located on the left side of the weld centerline is designated as HAZ 1, while the right side is designated as HAZ 2. In the original FBW, both HAZ 1 and HAZ 2 exhibited nearly identical average hardness values of approximately 260 HV. This region corresponds to the softened zone of the FBW rail joint, primarily attributed to the spheroidized microstructure. In contrast, the repaired FBW demonstrated consistent average hardness values of around 350 HV in both HAZ 1 and HAZ 2, which can be ascribed to the

DOI: https://doi.org/10.17509/ijost.v11i2.89691
p- ISSN 2528-1410 e- ISSN 2527-8045

formation of fine pearlite. These results indicate that the repair process successfully mitigated the weak zone of the original FBW by enhancing the hardness of the HAZ.

Figure 10 presents the hardness profile across the cross-section of a repaired FBW joint, measured at the centerline of the original FBW. Three distinct regions are identified: the weld metal (WM) of the repaired FBW, the HAZ of the repaired FBW, and the centerline of the original FBW. In the weld metal region, from the top surface to a depth of 5 mm, the hardness values ranged between approximately 300 and 350 HV, with an average of 330 HV. The HAZ of the repaired FBW exhibited relatively uniform hardness of around 350 HV, representing the highest values in the profile. By contrast, the hardness gradually decreased from 350 HV to about 250 HV at the weld centerline of the original FBW. These results indicate that the repair process effectively enhanced one of the weak areas of the FBW joint, namely the weld centerline, where the proeutectoid microstructure is commonly observed. Furthermore, the hardness profile is consistent with the corresponding microstructural observations. Similar trends were reported by Królicka et al., who found that hardness reduction at the weld centerline and adjacent HAZs also occurred in bainitic rail welded by FBW [36,37]. In their study, the lowest hardness was recorded in the HAZs, at around 270 HV, compared to approximately 380 HV in the bainitic steel base metal.

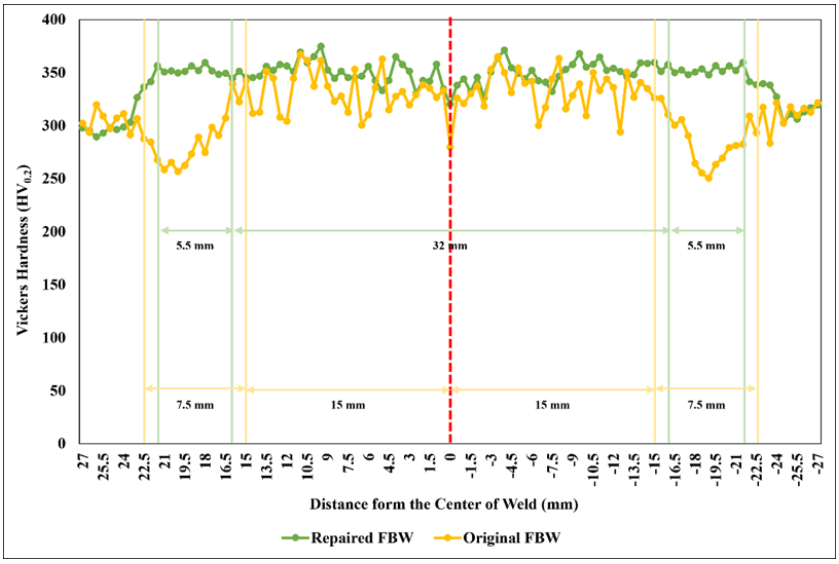

Figure 8. Comparison of hardness profiles across the weld cross-section of original FBW and repaired FBW.

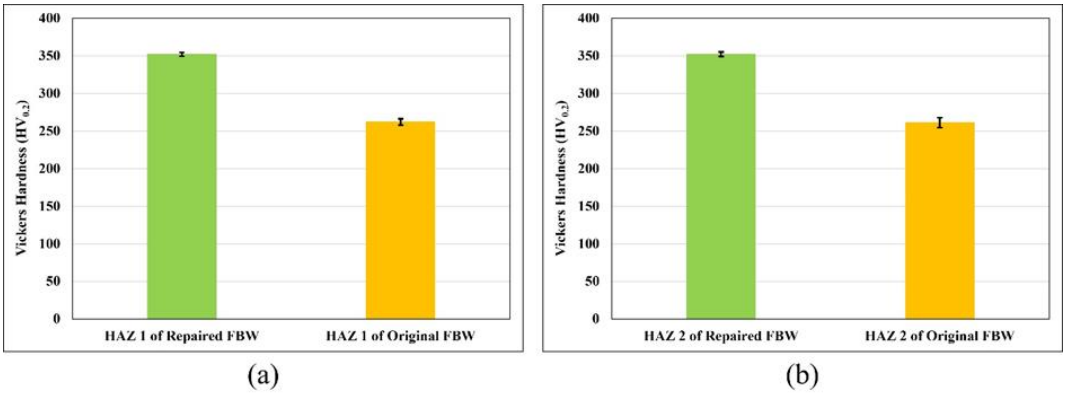

Figure 9. Average HAZ hardness of original and repaired FBW (a) HAZ 1 and (b) HAZ 2.

DOI: https://doi.org/10.17509/ijost.v11i2.89691
p- ISSN 2528-1410 e- ISSN 2527-8045

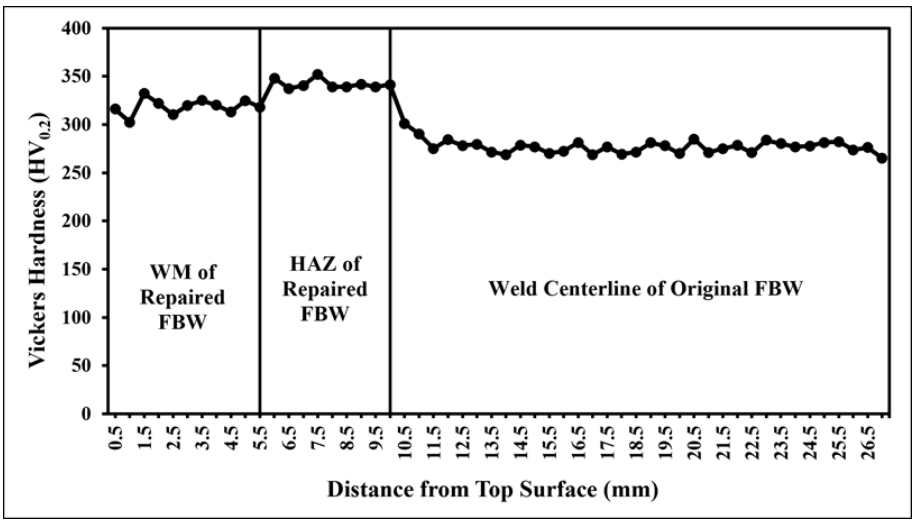

Figure 10. Hardness distribution and transitions of the repaired FBW obtained at the weld centerline of original FBW.

3.6. Wear Behavior

The wear behavior of both original and repaired FBW specimens was evaluated using a ball-on-disc wear tester. Parameters including the coefficient of friction, wear track width, and weight loss were examined. **Figure 11** shows the variation of the coefficient of friction as a function of the number of laps. Under all testing conditions, the coefficient of friction exhibited relatively similar trends. **Figure 12** presents the average coefficient of friction values for different test regions, which were 0.59 for the weld center of the original FBW, 0.55 for the HAZ of the original FBW, and 0.47 for the repaired FBW. These results demonstrate that the repaired FBW specimen consistently exhibited the lowest coefficient of friction among the three conditions, indicating an improvement in tribological performance after repair.

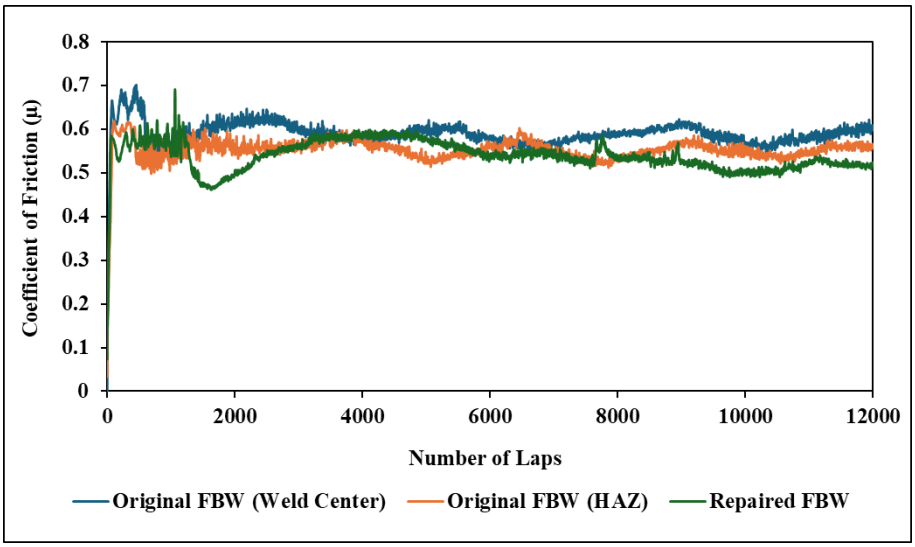

Figure 11. Coefficient of friction vs number of laps.

A scanning electron microscope (SEM) was used to measure the width of the wear tracks on the tested specimens. **Figure 13** shows the SEM images of wear tracks under different conditions. The measured wear track widths were 537 µm for the weld center of the original FBW, 557 µm for the HAZ of the original FBW, and 532 µm for the repaired FBW. Although minor variations were observed, the differences in wear track widths among the three

DOI: https://doi.org/10.17509/ijost.v11i2.89691
p- ISSN 2528-1410 e- ISSN 2527-8045

conditions were not significant, indicating that the repair process did not substantially affect the wear track dimensions.

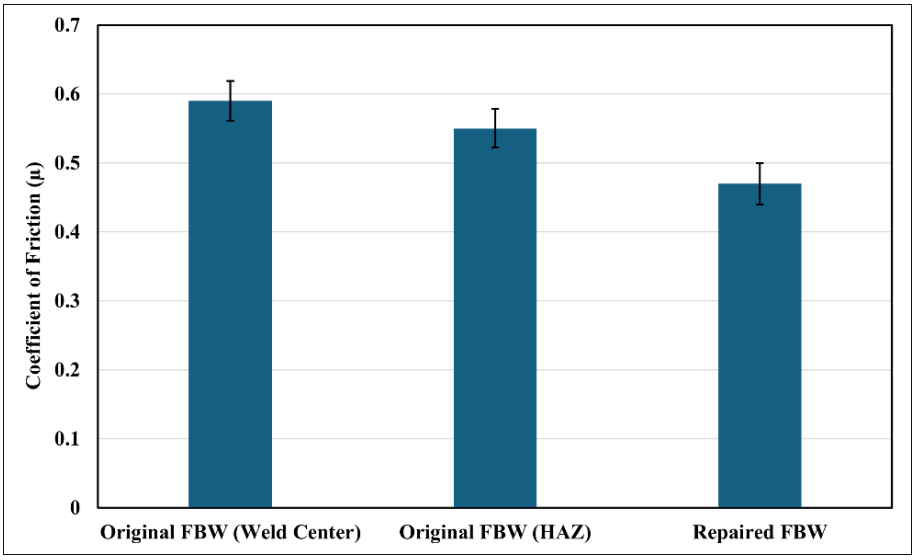

Figure 12. Average coefficient of friction.

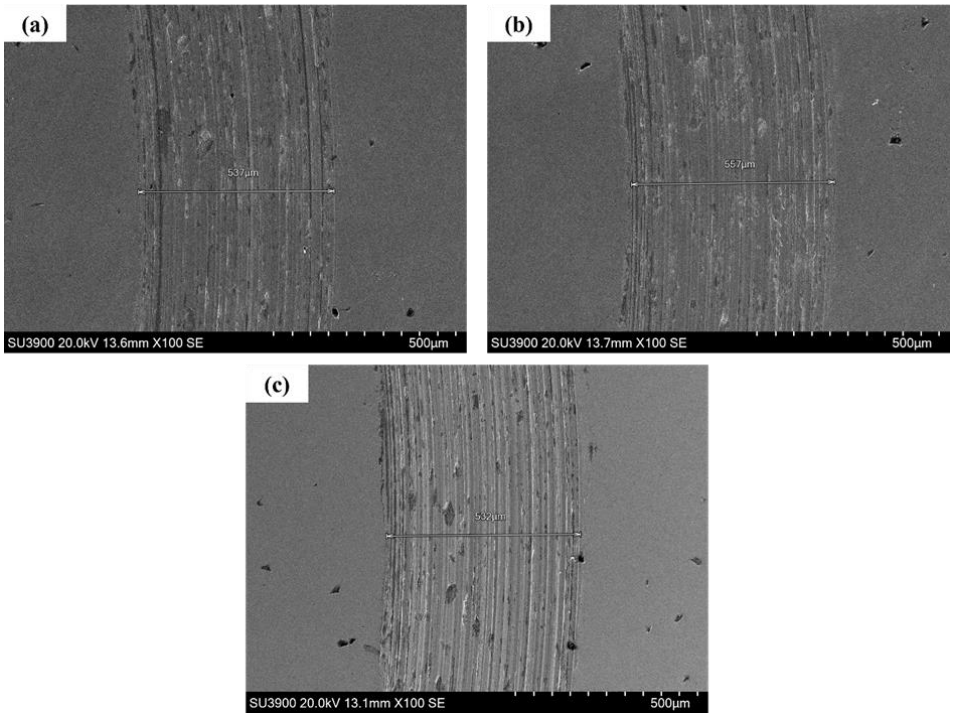

Figure 13. Wear track measurement (a) Original FBW (Weld Center), (b) Original FBW (HAZ) and (c) Repaired FBW.

Prior to and following the wear tests, the specimens were weighed to determine the corresponding weight loss. The average weight losses were measured as 6.5 µg/m for the weld center of the original FBW, 7.2 µg/m for the HAZ of the original FBW, and 5.9 µg/m for the repaired FBW. A comparison of the weight loss under different conditions is presented in **Figure 14**. The error bars in Figure 14 represent the standard deviation, based on the average results obtained from three specimens for each condition. Among the tested samples, the repaired FBW exhibited the lowest weight loss, whereas the HAZ of the original FBW demonstrated the highest weight loss.

DOI: https://doi.org/10.17509/ijost.v11i2.89691
p- ISSN 2528-1410 e- ISSN 2527-8045

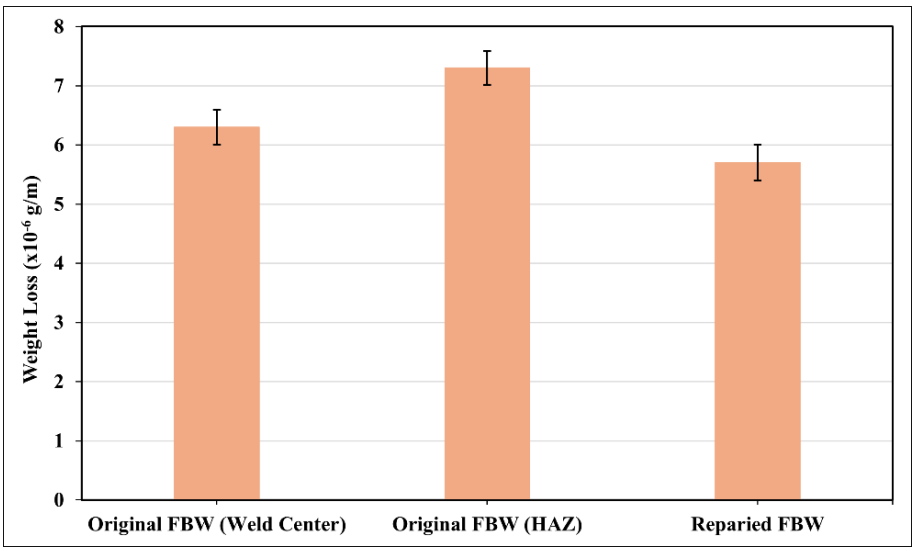

Figure 14. Weight loss after wear test

3.7. Worn Surface Morphology

The surface morphology of the worn specimens was examined using a scanning electron microscope (SEM), and the results are shown in **Figure 15**. For the original FBW, both at the weld center and the HAZ, the dominant wear mechanisms were micro-ploughing and micro-cutting. Spalling was also observed on the worn surface of the HAZ in the original FBW samples. The presence of deep abrasive furrows indicated the occurrence of abrasive wear, while numerous micro-fractures and pits were also detected on the worn surfaces.

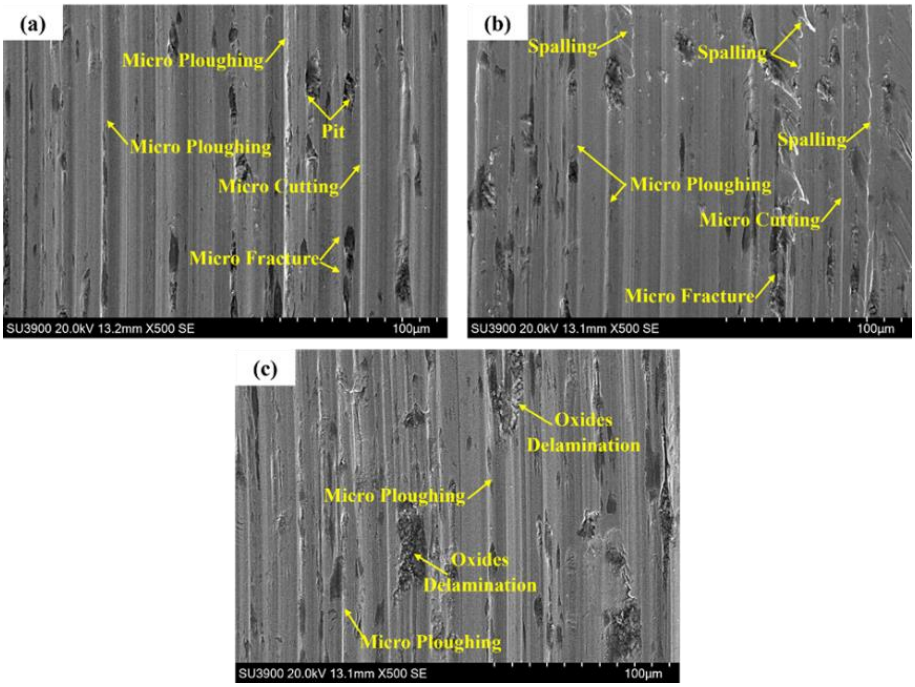

Figure 15. Worn surface morphology (a) Original FBW (Weld Center), (b) Original FBW (HAZ) and (c) Repaired FBW.

In contrast, the repaired FBW samples exhibited wear mechanisms primarily involving micro-ploughing and oxide delamination. Compared with the original FBW, the repaired specimens displayed shallower ploughing grooves. A significant amount of oxide debris was also observed, resulting from oxide delamination during wear testing. Overall, the wear

DOI: https://doi.org/10.17509/ijost.v11i2.89691
p- ISSN 2528-1410 e- ISSN 2527-8045

process of the repaired FBW involved a combination of abrasive and adhesive wear mechanisms, but with reduced severity compared to the original FBW.

4. CONCLUSION

This study demonstrated that repair welding can effectively enhance the properties of flash-butt welded (FBW) rail joints. The repair welding process refined the microstructure of both the heat-affected zone (HAZ) and the weld metal, resulting in increased hardness at the weld centerline and HAZ. Specifically, the HAZ of the repaired FBW exhibited a fine pearlite microstructure, while the weld metal predominantly consisted of acicular ferrite. Consequently, the repaired FBW displayed higher and more uniform hardness profiles across the weld region, with significant improvement observed in the HAZ and weld centerline, which were the weakest areas in the original FBW joints. In addition to the improvement in hardness, the repaired FBW also demonstrated enhanced wear resistance. Although the coefficients of friction and wear track widths were comparable between the original and repaired FBW, the repaired specimens exhibited shallower ploughing grooves, the presence of oxide debris from delamination, and a wear mechanism characterized by combined abrasive and adhesive behaviors. Overall, the repair process effectively strengthened the weak zones of the original FBW, particularly the weld centerline and HAZ, leading to improvements in both hardness and wear resistance. These findings highlight the potential of repair welding as a practical and efficient method to extend the service life of FBW rail joints.

5. ACKNOWLEDGMENT

This research was supported by Prince of Songkla University under the Postdoctoral Fellowship Program. The authors would like to thank Mr. Wissarut Sangwiman, Managing Director of Pearlite Construction Partnership (PCP) Company, Thailand, for supplying flash-butt welded rail joints for this research.

6. AUTHORS' NOTE

The authors declare that there is no conflict of interest regarding the publication of this article. The authors confirmed that the paper was free of plagiarism.

7. REFERENCES

[1] Skyttebol, A., Josefson, B. L., and Ringsberg, J. W. (2005). Fatigue crack growth in a welded rail under the influence of residual stresses. *Engineering Fracture Mechanics, 72*(2), 271–285.

[2] Lim, N.-H., Park, N.-H., and Kang, Y.-J. (2003). Stability of continuous welded rail track. *Computers and Structures, 81*(22–23), 2219–2236.

[3] Shen, M., Mei, L., Gong, F., Li, C., and Li, Q. (2024). Damage behaviour of rail flash-butt welding joints under controlled impact kinetic energy. *Wear, 552–553*, 205435.

[4] Jiang, W. J., Liu, C., He, C. G., Guo, J., Wang, W. J., and Liu, Q. Y. (2017). Investigation on impact wear and damage mechanism of railway rail weld joint and rail materials. *Wear, 376–377*, 1938–1946.

[5] Burapa, R., Oo, H. Z., Sangwiman, W., and Muangjunburee, P. (2024). Influences of preheating parameters on the quality of weld by thermite rail welding. *Materials Research Express, 11*(6), 066507.

DOI: https://doi.org/10.17509/ijost.v11i2.89691
p- ISSN 2528-1410 e- ISSN 2527-8045

[6] Wang, J., Ma, C., Han, J., Jiang, Z., and Linton, V. (2021). Acquisition of HSLA steel weld joints with excellent mechanical performance through flash butt welding physical simulation. *Materials Letters, 303*, 130511.

[7] Ozakgul, K., Piroglu, F., and Caglayan, O. (2015). An experimental investigation on flash butt welded rails. *Engineering Failure Analysis, 57*, 21–30.

[8] Xiao, G., Xiao, X., Guo, J., Wen, Z., and Jin, X. (2010). Track dynamic behavior at rail welds at high speed. *Acta Mechanica Sinica, 26*(3), 449–465.

[9] Wu, Y., Lun Pun, C., Su, H., Huang, P., Welsby, D., Mutton, P., and Yan, W. (2022). Numerical study on ratcheting performance of heavy haul rail flash-butt welds in curved tracks. *Engineering Failure Analysis, 140*, 106611.

[10] Bauri, L. F., Alves, L. H. D., Pereira, H. B., Tschiptschin, A. P., and Goldenstein, H. (2020). The role of welding parameters on the control of the microstructure and mechanical properties of rails welded using FBW. *Journal of Materials Research and Technology, 9*(4), 8058–8073.

[11] Mansouri, H., and Monshi, A. (2004). Microstructure and residual stress variations in weld zone of flash-butt welded railroads. *Science and Technology of Welding and Joining, 9*(3), 237–245.

[12] Tawfik, D., Mutton, P. J., and Chiu, W. K. (2008). Experimental and numerical investigations: Alleviating tensile residual stresses in flash-butt welds by localised rapid post-weld heat treatment. *Journal of Materials Processing Technology, 196*(1–3), 279–291.

[13] Shi, H. C., Shi, L. B., Ding, H. H., Wang, W. J., Jiang, W. J., Guo, J., and Liu, Q. Y. (2019). Influence of laser strengthening techniques on anti-wear and anti-fatigue properties of rail welding joint. *Engineering Failure Analysis, 101*, 72–85.

[14] Su, H., Li, J., Lai, Q., Pun, C. L., Mutton, P., Kan, Q., Kang, G., and Yan, W. (2020). Ratcheting behaviour of flash butt welds in heat-treated hypereutectoid steel rails under uniaxial and biaxial cyclic loadings. *International Journal of Mechanical Sciences, 176*, 105539.

[15] Lu, C., Nieto, J., Puy, I., Melendez, J., and Martínez-Esnaola, J. M. (2018). Fatigue prediction of rail welded joints. *International Journal of Fatigue, 113*, 78–87.

[16] Wang, Y., Zhou, H., Shi, Y., and Feng, B. (2012). Mechanical properties and fracture toughness of rail steels and thermite welds at low temperature. *International Journal of Minerals, Metallurgy, and Materials, 19*(5), 409–420.

[17] Losz, J. M. B., Saboury, S., and McNutt, T. M. (1995). Microstructural characterization of submerged-arc and gas-metal-arc weldments in HY-130 Steel. *ISIJ International, 35*(1), 71–78.

[18] Pereira, H. B., Echeverri, E. A. A., Alves, L. H. D., and Goldenstein, H. (2022). Evaluation of the effect of heat input and cooling rate of rail flash-butt welding using finite element method simulation. *Soldagem and Inspeção*, *27*, e2701.

[19] Nishikawa, L. P., and Goldenstein, H. (2019). Divorced eutectoid on heat-affected zone of welded pearlitic rails. *JOM, 71*(2), 815–823.

[20] Pavlina, E. J., and Van Tyne, C. J. (2008). Correlation of yield strength and tensile strength with hardness for steels. *Journal of Materials Engineering and Performance, 17*(6), 888–893.

[21] Porcaro, R. R., Faria, G. L., Godefroid, L. B., Apolonio, G. R., Cândido, L. C., and Pinto, E. S. (2019). Microstructure and mechanical properties of a flash butt welded pearlitic rail. *Journal of Materials Processing Technology, 270*, 20–27.

DOI: https://doi.org/10.17509/ijost.v11i2.89691
p- ISSN 2528-1410 e- ISSN 2527-8045

[22] Steenbergen, M., and Dollevoet, R. (2013). On the mechanism of squat formation on train rails – Part II: Growth. *International Journal of Fatigue, 47*, 373–381.
[23] Fegredo, D. M., Kalousek, J., and Shehata, M. T. (1993). The effect of progressive minor spheroidization on the dry-wear rates of a standard carbon and a Cr-Mo alloy rail steel. *Wear, 161*(1–2), 29–40.
[24] Mutton, P., Cookson, J., Qiu, C., and Welsby, D. (2016). Microstructural characterisation of rolling contact fatigue damage in flashbutt welds. *Wear, 366–367*, 368–377.
[25] Steenbergen, M. (2021). On the genesis of squat-type defects on rails–Toward a unified explanation. *Wear*, *478*, 203906.
[26] Oo, H. Z., and Muangjunburee, P. (2023). Improving microstructure and hardness of softening area at HAZ of thermite welding on rail running surface. *Materials Today Communications, 34*, 105485.
[27] Oo, H. Z., and Muangjunburee, P. (2024). Hardfacing of thermite welded rail by flux-cored arc welding. *Wear, 546*, 205314.
[28] Su, H., Pun, C. L., Mutton, P., Kan, Q., Kang, G., and Yan, W. (2021). Numerical study on the ratcheting performance of rail flash butt welds in heavy haul operations. *International Journal of Mechanical Sciences, 199*, 106434.
[29] Abson, D. J., and Pargeter, R. J. (1986). Factors influencing as-deposited strength, microstructure, and toughness of manual metal arc welds suitable for C-Mn steel fabrications. *International Metals Reviews, 31*(1), 141–196.
[30] Madariaga, I., Gutierrez, I., and Bhadeshia, H. K. D. H. (2001). Acicular ferrite morphologies in a medium-carbon microalloyed steel. *Metallurgical and Materials Transactions A, 32*(9), 2187–2197.
[31] Loder, D., Michelic, S. K., and Bernhard, C. (2016). Acicular ferrite formation and its influencing factors-a review. *Journal of Materials Science Research, 6*(1), 24.
[32] Muangjunburee, P., Oo, H. Z., Rahim, S. Z. A., and Srikarun, B. (2024). Effects of heat input and preheating temperature on the microstructure and hardness of repairing the heat-affected zone of thermite welded rail head surface. *Indonesian Journal of Science and Technology, 9*(2), 421–440.
[33] Krolicka, A., Lesiuk, G., Radwański, K., Kuziak, R., Janik, A., Mech, R., and Zygmunt, T. (2021). Comparison of fatigue crack growth rate: Pearlitic rail versus bainitic rail. *International Journal of Fatigue*, *149*, 106280.
[34] Masoumi, M., Lima, N. B. de, Tressia, G., Sinatora, A., and Goldenstein, H. (2019). Microstructure and crystallographic orientation evolutions below the superficial white layer of a used pearlitic rail. *Journal of Materials Research and Technology, 8*(6), 6275–6288.
[35] Fei, J., Zhou, G., Zhou, J., Zhou, X., Li, Z., Zuo, D., and Wu, R. (2023). Research on the effect of pearlite lamellar spacing on rolling contact wear behavior of U75V rail steel. *Metals, 13*(2), 237.
[36] Krolicka, A., Radwański, K., Kuziak, R., Zygmunt, T., and Ambroziak, A. (2020). Microstructure-based approach to the evaluation of welded joints of bainitic rails designed for high-speed railways. *Journal of Constructional Steel Research*, *175*, 106372.
[37] Krolicka, A., Zak, A., Kuziak, R., Radwanski, K., and Ambroziak, A. (2021). Decomposition mechanisms of continuously cooled bainitic rail in the critical heat-Affected zone of a flash-butt welded joints. *Materials Science- Poland, 39*(4), 615–625.

DOI: https://doi.org/10.17509/ijost.v11i2.89691
p- ISSN 2528-1410 e- ISSN 2527-8045